Mutual Inductance of Noncoaxial Circular Coils with Constant Current Density

Ki-Bong Kim, *Member, IEEE*, Enrico Levi, *Life Senior Member, IEEE*, Zivan Zabar, *Senior Member, IEEE*, and Leo Birenbaum, *Life Senior Member, IEEE*

***Abstract*—The purpose of this paper is to determine the mutual inductance between two noncoaxial circular coils. In many cases, such as coil guns or tubular linear motors, one of them is fixed while the other one is moving, and if not supported, its axis may not coincide with that of the fixed coil. This paper presents a method for the calculation of the mutual inductance in the case of noncoaxial coupled coils, the characteristics of this inductance, and experimental results. The computation is based on complete elliptic integrals and on mesh-matrix technique. The method enables one to obtain accurate results from a relatively simple procedure and calculation program.**

***Index Terms*—Mutual inductance, noncoaxial coils.**

I. Introduction

CIRCULAR coils are widely used in various electromagnetic applications such as coil guns and tubular linear motors. When the machines are of the induction type, the mutual inductance between primary and secondary is the principal parameter determining the current induced in the secondary winding, and the centering and propelling forces [1], [2]. If the machine is such that its secondary is not supported by any means, the axis of the secondary winding may not coincide with the axis of the primary. In this case, the mutual inductance between the primary and secondary coils is not the same as in the coaxial case. As a result, if the machine is of the induction type, the current induced in the secondary may also be expected to be different. There is an extensive literature dealing with the calculation of inductance, but the portion on mutual inductance is mainly concerned with the axially symmetric case [3], [4]. In contrast, the work presented here deals with the asymmetric case. The need for an accurate knowledge of the mutual inductance between noncoaxial coils emerges when it is required to analyze and understand the behavior of transversely movable secondary conductors, such as the projectile in a coil gun. Most of the calculations for mutual inductance start by first obtaining the vector magnetic potential. Typically, formulas based on the Biot–Savart law are used in analysis of magnetic field [5]–[18].

Grover [19] is an encyclopedic source of information, numerical and otherwise, for inductances of coils of various shapes, and includes some early material on mutual inductance between noncoaxial circular coils. The configuration of the coils used in this analysis is drawn in Fig. 1. The primary and secondary coils have the dimensions shown in the picture: the thickness of the secondary H_S is assumed to be relatively small, that is, less than the depth of penetration δ if it is a single-turn solenoid conductor; otherwise, if it is a multiturn coil, the wire diameter is assumed to be less than δ. The primary coils of tubular linear motors or coil guns usually have multiturn windings to match the impedance level of the source [2]. Therefore, it is reasonable to assume that the current distribution in the primary coil is uniform. In this analysis, the number of turns in the primary coil is N_p, and that in the secondary coil is N_s, the current in the primary winding is I_p, and the off-center distance is y.

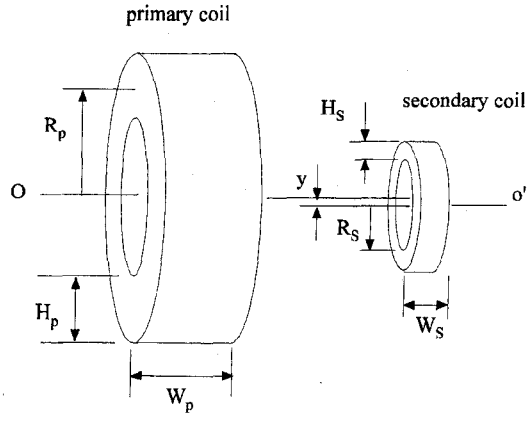

Fig. 1. Configuration of the primary coil and the secondary coil.

II. Calculation with Complete Elliptic Integrals and Mesh-Matrix Method

In order to account for the finite dimensions of the coils, the primary and secondary are considered to be subdivided into meshes of filamentary coils as shown in Fig. 2 [6], [20], [22]. In this figure, the cross-sectional area of the primary coil is divided into $(2M + 1)$ by $(2N + 1)$ cells, and that of the secondary coil into $(2m + 1)$ by $(2n + 1)$ cells. These cells need not correspond to the actual turns of the coils. If the cross section of the coils is not rectangular, e.g., circular, the current densities in nonexisting elements can be regarded as zero when the calculation is performed. Each cell in the primary coil contains one filament, and the current density in the coil cross section is assumed to be uniform, so that the filament currents are all equal. Hence, the total magnetic flux

Manuscript received May 14, 1995; revised November 12, 1996.

K.-B. Kim is with the Living System R&D Center, SamSung Electronics Co., Suwon-city, Korea.

E. Levi, Z. Zabar, and L. Birenbaum are with the Electrical Engineering Department, Polytechnic University, Brooklyn, NY 11201 USA.

Publisher Item Identifier S 0018-9464(97)04902-9.

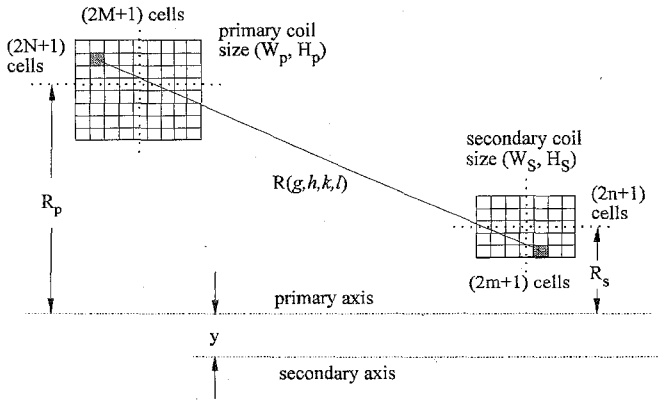

Fig. 2. Configuration of mesh matrix.

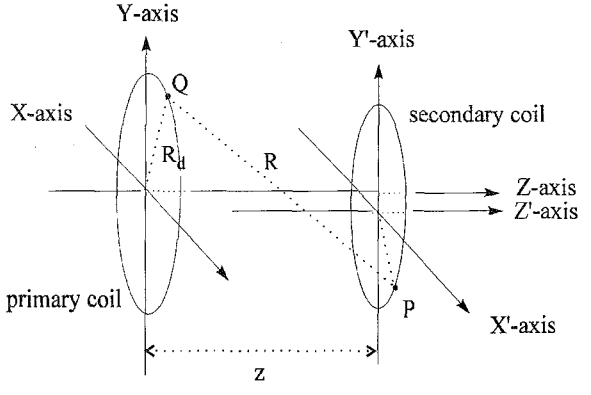

Fig. 3. Side view of the two filamentary coils.

linked with any secondary filament is the sum of the magnetic fluxes due to all of the filamentary cells in the primary coil.

The vector magnetic potential at point P on the secondary filament j due to the entire length of the primary filament i has a tangential component only, and it can be expressed as

$$A_\phi \cdot \tilde{\boldsymbol{a}}_\phi = \frac{\mu_0 I_i}{4\pi} \oint \frac{d\ell_2}{R} = \frac{\mu_0 I_i}{2\pi} \int_0^\pi \frac{R_p \cos\phi_1}{\left(R_p^2 + r^2 + z^2 - 2R_p r\cos\phi_1\right)^{1/2}} d\phi_1 \cdot \boldsymbol{a}_\phi \tag{1}$$

where R is the distance between point P and point Q, r is the distance between the primary coil origin O and point P on the secondary coil, ϕ is the angular coordinate, and z is the axial distance between the primary and secondary filaments.

Figs. 3 and 4 show the dimensions and variables to be used for the calculation of the magnetic flux and mutual inductance for a pair of filamentary coils. From Figs. 3 and 4, one can find that

$$r = [(y + R_s\cos\phi_2)^2 + (R_s\sin\phi_2)^2]^{1/2}. \tag{2}$$

Letting $\phi_1 = \pi + 2\theta$ so that $d\phi_1 = 2\,d\theta$ and $\cos\phi_1 = 2\sin^2\theta - 1$, then

$$A_\phi = \frac{\mu_0 R_p I_i}{\pi} \int_0^{\pi/2} \frac{(2\sin^2\theta - 1)\,d\theta}{[(R_p + r)^2 + z^2 - 4R_p r\sin^2\theta]^{1/2}}. \tag{3}$$

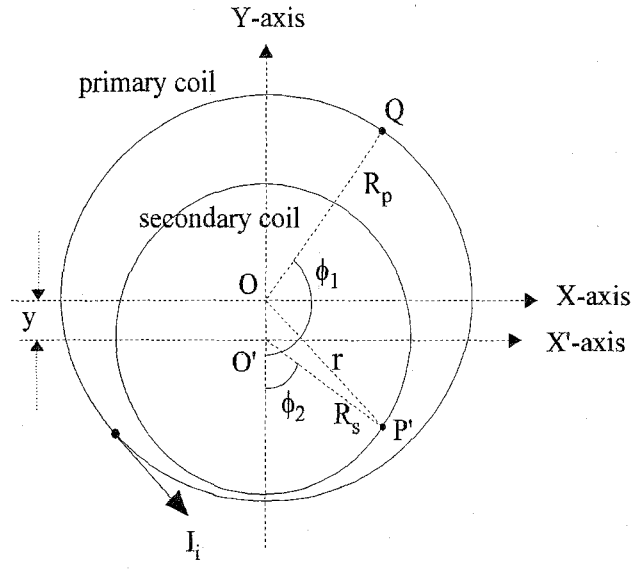

Fig. 4. Front view of the two filamentary coils.

Using the modulus κ, one can rearrange the integrand to get the following expression for the vector magnetic potential:

$$A_\phi = \frac{\mu_0 I_i}{\pi\kappa}\left(\frac{R_p}{r}\right)^{1/2}\left[\left(1 - \frac{1}{2}\kappa^2\right)K(\kappa) - E(\kappa)\right] \tag{4}$$

where E and K are the complete elliptic integrals of the first and second kind, respectively [21].

$$E = \int_0^{\pi/2} (1 - \kappa^2\sin^2\vartheta)^{1/2}\,d\vartheta \tag{5}$$

$$K = \int_0^{\pi/2} \frac{1}{(1 - \kappa^2\sin^2\vartheta)^{1/2}}\,d\vartheta \tag{6}$$

and the modulus is

$$\kappa = \left[\frac{4R_p r}{(R_p + r)^2 + z^2}\right]^{1/2}. \tag{7}$$

Substituting the modulus into (4), one can find the final formula for the vector magnetic potential used in this paper

$$A_\phi = \frac{\mu_0 I_i}{2\pi r}[(R_p + r)^2 + z^2]^{1/2}\left[\left(1 - \frac{1}{2}\kappa^2\right)K(\kappa) - E(\kappa)\right]. \tag{8}$$

Introducing the relationship between flux density $\boldsymbol{B}$ and vector magnetic potential $\boldsymbol{A}$, $\boldsymbol{B} = \nabla \times \boldsymbol{A}$, and Stokes's theorem, one can write

$$\phi_{ij} = \iint_{s_{2j}} (\nabla \times \boldsymbol{A}_{ij}) \cdot d\boldsymbol{s}_{2j} = \oint_{\ell_{2j}} \boldsymbol{A}_{ij} \cdot d\ell_{2j} \tag{9}$$

where ℓ_{2j} is the length at the loop of the secondary filament j. Using this equation, one can rewrite (9) as

$$\phi_{ij} = \frac{\mu_0 I_i R_s}{2\pi r}\int_{\phi_2=0}^{2\pi} [(R_p + r)^2 + z^2]^{1/2} \times \left[\left(1 - \frac{1}{2}\kappa^2\right)K(\kappa) - E(\kappa)\right] d\phi_2. \tag{10}$$

The mutual inductance between the composite primary and secondary coils may be calculated by summing up those

between the primary and secondary filaments. The mutual inductance between a primary filament $i(g,h)$ and a secondary filament $j(k,l)$, where g and k denote the column of the cells and h and ℓ denote the row, is

$$M_{ij} = \frac{\lambda_{ij}}{I_i} \tag{11}$$

where λ_{ij} is the magnetic flux linking the secondary filament $j(k,l)$ due to the current I_i in the primary filament $i(g,h)$.

Thus, the mutual inductance between the pair of filamentary unit turn coils can be found as

$$M_{ij} = \frac{\mu_0 R_s}{2\pi r} \int_{\phi_2=0}^{2\pi} [(R_p + r)^2 + z^2]^{1/2} \times \left[\left(1 - \frac{1}{2}\kappa^2\right)K(\kappa) - E(\kappa)\right] d\phi_2. \tag{12}$$

To determine the mutual inductance M_{12} between the composite primary and secondary coils, the following reasoning is employed. The magnetic flux linking the secondary coil filament j, due to the entire set of primary current filaments of which current density with the previous assumption of uniform distribution being

$$I_i = \frac{N_p I_p}{(2M+1)(2N+1)}$$

is given by $\sum_i \phi_{ij}$, and the total magnetic flux linking all of the secondary filaments is given by $\sum_j (\sum_i \phi_{ij})$. Since each secondary filament is only a fraction

$$\frac{N_s}{(2m+1)(2n+1)}$$

of the secondary coil turns, the flux linkage λ with the secondary winding is given by

$$\lambda = \frac{N_s}{(2m+1)(2n+1)} \sum_j \left(\sum_i \phi_{ij}\right) = \frac{N_s}{(2m+1)(2n+1)} \sum_j \left(\sum_i I_i M_{ij}\right). \tag{13}$$

Hence M_{12} is given by

$$M_{12} = \frac{\lambda_{12}}{I_P} = \frac{I_i}{I_P} \frac{N_s}{(2m+1)(2n+1)} \sum_j \left(\sum_i M_{ij}\right) = \frac{N_P N_s}{(2M+1)(2N+1)(2m+1)(2n+1)} \times \sum_j \left(\sum_i M_{ij}\right). \tag{14}$$

To evaluate M_{12}, each function in (14) must be expressed in terms of the corresponding coordinates as follows:

$$r_\ell^2 = (R_{s\ell} \cos\phi_2 + y)^2 + (R_{s\ell} \sin\phi_2)^2 \tag{15}$$

$$R_{ph} = R_p + \frac{H_p}{2N+1} h \tag{16}$$

$$R_{s\ell} = R_s + \frac{H_s}{2n+1} \ell \tag{17}$$

$$z_{g,k} = z - \frac{W_p}{2M+1} g + \frac{W_s}{2m+1} k \tag{18}$$

and the modulus

$$\kappa_{g,h,k,l} = \left[\frac{4R_{ph} r_\ell}{(R_{ph} + r_\ell)^2 + z_{g,k}^2}\right]^{1/2}. \tag{19}$$

From (14), the net mutual inductance can be re-expressed as

$$M_{12} = \frac{N_P N_S}{(2M+1)(2N+1)(2m+1)(2n+1)} \times \sum_{g=-M}^{M} \sum_{h=-N}^{N} \sum_{k=-m}^{m} \sum_{l=-n}^{n} M_{ij(g,h,k,l)} \tag{20}$$

where $M_{ij(g,h,k,l)}$ is as shown in (12). Equation (20) is the final form for the mutual inductance between two noncoaxial circular coils.

III. Calculation Results

A. Calculation 1: ($N_p = 150, N_s = 50$)

For later comparison to experimental results in experiments 1, 2, and 3, several calculations were carried out. The calculation results vary depending on the number of meshes in the coils. However, the changes of the calculation results become smaller and smaller as the number of meshes is increased. In order to save calculation time, one has to limit the number of meshes. The following results, corresponding to the experiment 1, were obtained by letting the number of meshes in the primary be 5 by 5, i.e., $M = N = 2$, and, in the secondary, 3 by 3, i.e., $m = n = 1$. The coil dimensions were as follows.

1) *Primary Coil:* $D_p = 85$ mm, $R_p = 42.5$ mm, $W_p = 10$ mm, $H_p = 10$ mm, $N_p = 150$.
2) *Secondary Coil:* $D_s = 40$ mm, $R_s = 20.0$ mm, $W_s = 4$ mm, $H_s = 4$ mm, $N_s = 50$.

D_p and D_s are the diameters of the primary and secondary coils, respectively.

The dependence of the mutual inductance on the separation distance z was calculated for several values of the off-center distance y as shown in Fig. 5; the off-center distances are $y = 0.0, 1.0, 2.5, 5.0, 7.0$, and 10.0 mm, the last being the uppermost curve.

B. Calculation 2: ($N_p = 10, N_s = 1$)

Another calculation, which corresponds to experiment 2, was done with the following coil dimensions.

1) *Primary Coil:* $D_p = 39.7$ mm, $W_p = 30.2$ mm, $H_p = 22.0$ mm, $N_p = 10$.
2) *Secondary Coil:* $D_s = 24.6$ mm, $W_s = 10.0$ mm, $H_s = 1.65$ mm, $N_s = 1$.

The mutual inductance was calculated for different values of the off-center distance y. In Fig. 6, the off-center distances are $y = 0.0, 1.0, 2.5, 5.0$, and 7.0 mm, the last being the uppermost curve.

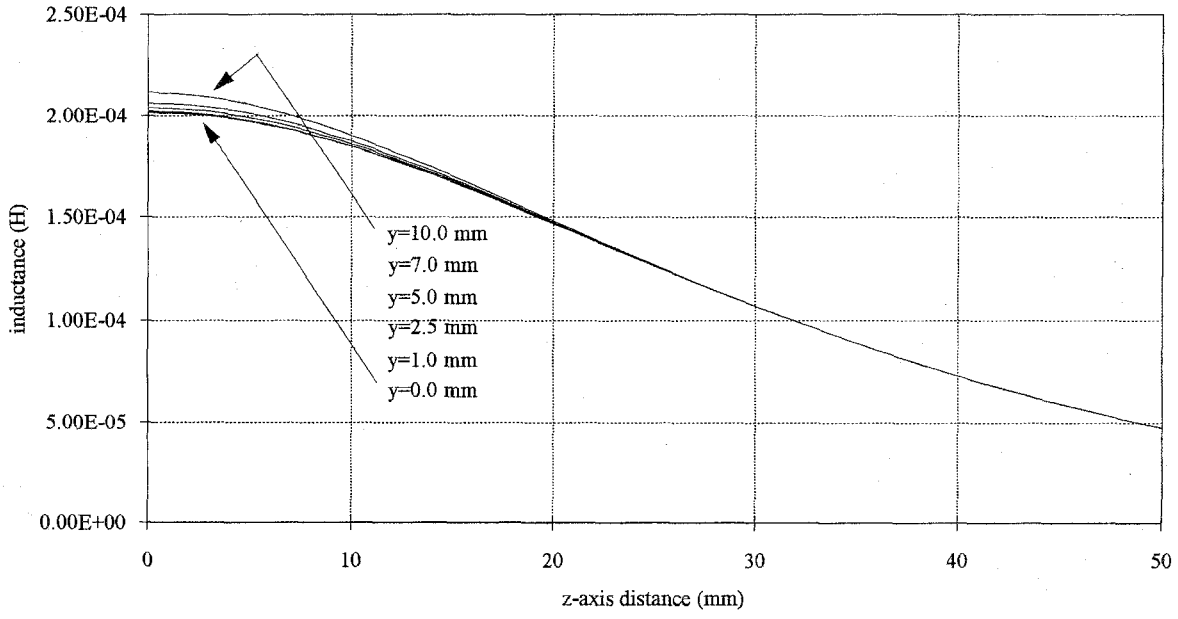

Fig. 5. Mutual inductance as a function of axial distance z, with the off-axis displacement y as a parameter.

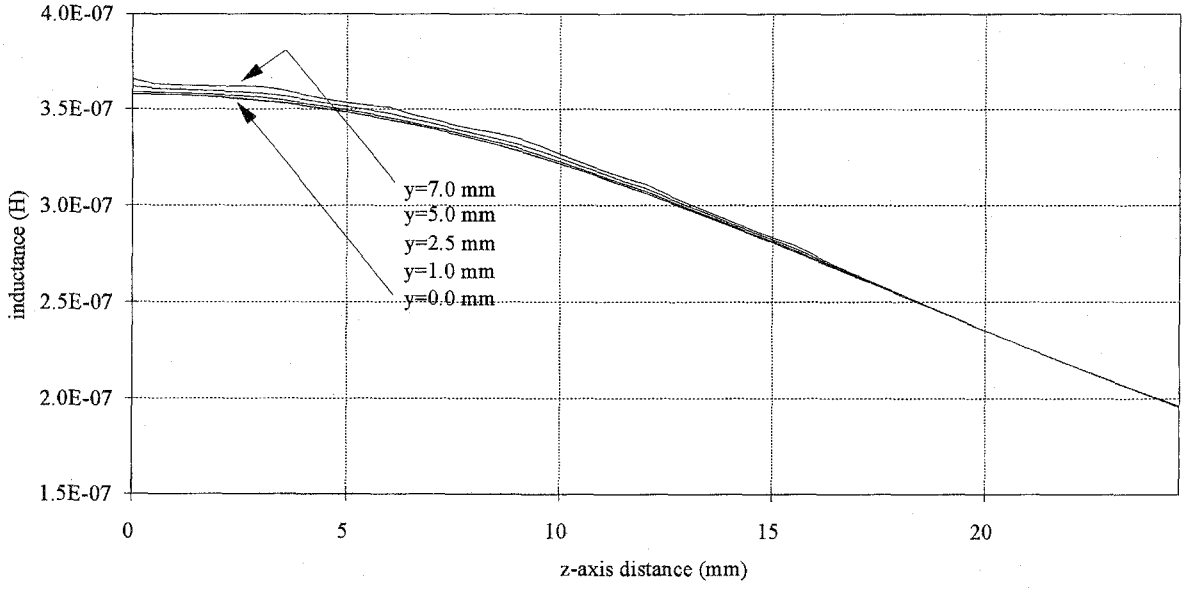

Fig. 6. Mutual inductance as a function of axial distance z, with the off-axis displacement y as a parameter.

C. Enlarged Plot: $(z = 0, N_p = 10, N_s = 1)$

In Figs. 5 and 6, it is seen that, for $z = 0$, the mutual inductance increases as the off-center distance y increases. This increment is shown in greater detail in Fig. 7. With the coil dimensions of calculation 2, the mutual inductance as a function of off-center distance y for $z = 0$ is plotted as y is varied from 0.0 to 7.2 mm.

From Figs. 5–7, it can be concluded that the mutual inductance increases as the off-center distance y gets larger. However, if the air gap is relatively small, the fractional change in the mutual inductance is not very significant.

IV. Experimental Measurements

The computer calculations were compared to the results of actual experiments in the laboratory. Three experiments were performed with the setup shown in Figs. 8 and 9. If a sinusoidal ac current is applied to the primary coil, the change in the primary coil flux induces a voltage in the secondary coil. Assuming plane wave propagation in the secondary conductor, the electric field may be expressed as

$$E_\phi = E_0 \exp\left[-(1+j)\left(\frac{\omega\mu\sigma}{2}\right)^{1/2} r\right]. \tag{21}$$

Since the secondary conductors are taken to be good conductors, the skin depth is expressible as

$$\delta = \frac{1}{\sqrt{\pi f \mu\sigma}} \tag{22}$$

where μ is the permeability and σ is the conductivity.

With a frequency of 1 kHz (as used in experiments 1–3) applied by the ac power source, (22) gives a skin depth of

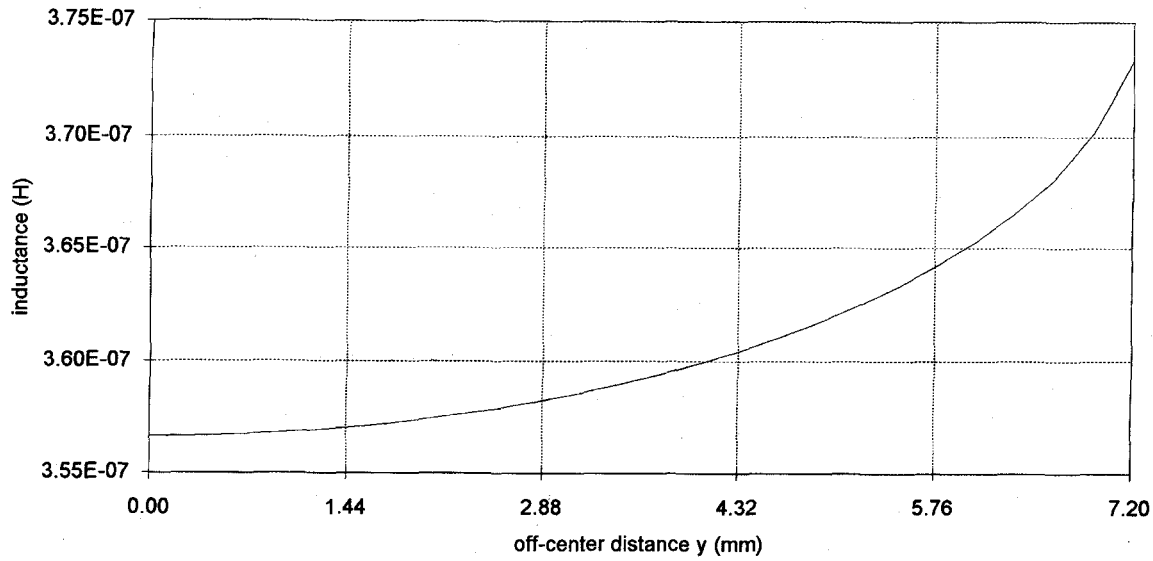

Fig. 7. Mutual inductance as a function of the off-axis displacement y, with axial distance $z = 0$.

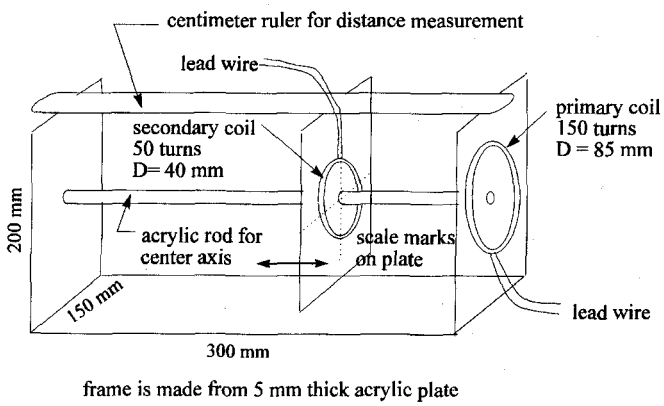

Fig. 8. Experimental setup.

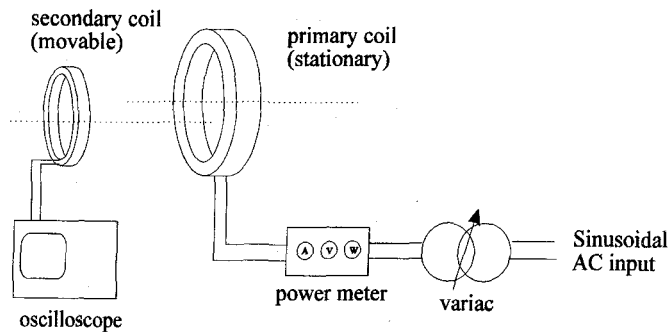

Fig. 9. Instrumentation.

2.575 mm for aluminum ($\rho = 2.62 \times 10^{-8}\ \Omega \cdot$ m) and 2.09 mm for copper ($\rho = 1.724 \times 10^{-8}\ \Omega \cdot$ m). If the frequencies are 60, 1250, and 2500 Hz, skin depth for aluminum conductor would be 10.5, 2.3, and 1.63 mm, respectively. These values are to be compared to the secondary copper wire diameter of 0.2 mm in experiments 1 and 3, and an aluminum tube thickness of 1.6 mm in experiment 2. The internal impedance of the oscilloscope was set to be 1 MΩ, while the secondary coil had a resistance of less than 0.2 Ω, and an inductance of 0.3 mH. Thus, the induced voltage in the secondary coil is given by

$$E_2 = 2\pi f M_{12} I_P \tag{23}$$

and the mutual inductance is

$$M_{12} = \frac{E_2}{2\pi f I_P} \tag{24}$$

where E_2 and I_P are rms values.

A. Experiment 1

The experiment was done at 1 kHz with the setup shown in Figs. 8 and 9. The primary coil was fixed to one end plate of the frame so that it could not move. Another coil, the secondary, was attached to the movable plate in the middle of the frame. It could be shifted horizontally, and also could be moved to vary the off-center distance. Fig. 9 represents the equipment for the measurement of the mutual inductance. An ac current input was applied to the primary coil and was measured by an ammeter in the power meter. The induced voltage in the secondary coil was measured by the oscilloscope.

For the first experiment, a primary coil of 85 mm average diameter having 150 turns of 0.65-mm-diameter copper wire was selected; the secondary coil had an average diameter of 40 mm and had 50 turns of 0.20-mm-diameter copper wire. Results of the experiment are listed in Table I.

The discrepancy between calculated and experimental results does not exceed 6%.

B. Experiment 2

The results of a second experiment performed at 1 kHz with a single-turn secondary coil are listed in Table II. The secondary coil was a 2024 T-30 reinforced aluminum ring having a diameter of 1 inch, a width of 10 mm, and a thickness of 1.6 mm. It was cut at one end to make a very small air gap to connect electric wire for measurement of the induced

TABLE I
SUMMARY OF EXPERIMENT 1 RESULTS

no.	z distance (cm)	mutual inductance (μH) $y = 0$ mm	$y = 3$ mm	$y = 7$ mm
1	0.0	195	200	204
2	0.5	190	192	200
3	1.0	180	181	181
4	2.0	122	122	122
5	3.0	79	79	79
6	4.0	50	50	50

TABLE II
SUMMARY OF EXPERIMENT 2 RESULTS

no.	distance z(cm)	mutual inductance (μH)
1	0.0	0.36
2	0.5	0.34
3	1.0	0.30
4	1.5	0.27
5	2.0	0.22
6	2.5	0.18
7	3.0	0.16
8	3.5	0.11
9	4.0	0.08
10	4.5	0.07
11	5.0	0.05

voltage. The primary coil was formed of ten layers of solid copper bar, which made its cross-sectional dimension 30.2 mm $\times$ 22.0 mm. The coils were placed with an off-center distance of 1 mm, which is the maximum air gap of the model-3 linear induction-type coil gun at Polytechnic University. Here, the discrepancy between calculated and experimental results does not exceed 7%.

C. Experiment 3

In Section III-C, it was shown that the mutual inductance increases as the off-center distance gets larger. However, in experiments 1 and 2, the changes of the mutual inductance with off-center distance y were quite small. In order to determine the nature of this dependence clearly, a third experiment was performed (also at 1 kHz) with a primary coil, wound with a larger radius, $R_p = 77.0$ mm, using 60 turns of 2-mm-diameter copper wire . The secondary coil was moved up and down in a radial direction, while the primary coil remained fixed. The longitudinal distance between the primary coil and the secondary coil z was zero. The results of this experiment are listed in Table III.

From Table III, it can be seen that the mutual inductance increases as the off-center distance increases, as indicated in Figs. 3 and 4. The discrepancy was less than 4%.

TABLE III
SUMMARY OF EXPERIMENT 3 RESULTS

No.	y (cm)	mutual inductance (μH)
1	0.00	1.81
2	1.25	1.87
3	2.54	1.98
4	3.75	2.15

V. CONCLUSION

A procedure has been provided for the accurate calculation of the mutual inductance of axially and laterally displaced circular coils; the procedure has been verified experimentally. It was shown in Figs. 4–6, and proved by the experiments, that the mutual inductance increases as the off-center distance gets bigger. The physical meaning of this result is that, with a dynamically oscillating secondary coil, the induced current and the restoring force [1], [22] in the secondary coil get bigger as the secondary coil approaches close to the primary coil. The maximum off-center distance in induction circular coil machines is limited by the air gap distance of the machines. Therefore, it is obvious that the effect of the mutual inductance increment in small air gap machines is less than that in machines with large air gaps. It should be noted, however, that the restoring force is proportional to the gradient of the mutual inductance and, as can be seen from Fig. 7, this gradient increases rapidly as the off-center distance increases and, therefore, the minimal air gap distance decreases. In all cases, the error in the calculated results is well within engineering tolerance. In all cases, the discrepancy between the calculated and experimental results did not exceed 7%.

REFERENCES

[1] K. B. Kim, Z. Zabar, E. Levi, and L. Birenbaum, "In-bore projectile dynamics in the linear induction launcher (LIL). Part 1: Oscillations," *IEEE Trans. Magn.*, vol. 31, pp. 484–488, Jan. 1995.

[2] Z. Zabar, "Novel schemes for electromagnetic launchers," final rep., SDIO/IST, Polytechnic Univ., Jan. 30, 1991 (Contract DASG60-88-C-0047).

[3] M. W. Garrett, "Calculation of fields, force and mutual inductances of current systems by elliptic integrals," *J. Appl. Phys.*, vol. 34, no. 9, pp. 2567–2573, Sept. 1963.

[4] T. H. Fawzi and P. E. Burke, "The accurate computation of self- and mutual inductances of circular coils," *IEEE Trans. Power Appar. Syst.*, vol. PAS-97, pp. 464–468, Mar./Apr. 1978.

[5] Z. X. Feng, "The treatment of singularities in calculation of magnetic field by using integral method," *IEEE Trans. Magn.*, vol. MAG-21, no. 6, pp. 2207–2210, Nov. 1985.

[6] B. Azzerboni, E. Cardelli, M. Raugi, and A. Tellini, "Some remarks on the current filament modeling of electromagnetic launchers," *IEEE Trans. Magn.*, vol. 29, pp. 643–648, Jan. 1993.

[7] B. Azzerboni, E. Cardelli, M. Raugi, A. Tellini, and G. Tina, "Magnetic field evaluation for thick annular conductors," *IEEE Trans. Magn.*, vol. 29, pp. 2090–2094, May 1993.

[8] B. Azzerboni, E. Cardelli, M. Raugi, G. Tina, and A. Tellini, "Analytical expressions for magnetic field from finite curved conductors," *IEEE Trans. Magn.*, vol. 27, pp. 750–757, Mar. 1991.

[9] B. Azzerboni, E. Cardelli, and A. Tellini, "Computation of the magnetic field in massive conductor system," *IEEE Trans. Magn.*, vol. 25, Nov. 1989.

[10] W. A. Perkins and J. C. Brown, "MAFCO—Magnet field code for handling general current elements in three dimensions," *J. Appl. Phys.*, vol. 35, pp. 3337–3343, 1964.

[11] V. I. Danilov and M. Ianovici, "Magnetic field of thick finite dc solenoids," *Nucl. Instrum. Meth.*, vol. 94, pp. 541–550, 1971.

[12] I. R. Ciric, "Simple analytical expressions for the magnetic field of current coils," *IEEE Trans. Magn.*, vol. 27, pp. 669–673, Jan. 1991.

[13] L. Urankar, "Vector potential and magnetic field of current-carrying finite arc segment in analytical form. Part I: Filament approximation," *IEEE Trans. Magn.*, vol. MAG-16, pp. 1283–1288, Sept. 1980.

[14] ——, "Vector potential and magnetic field of current-carrying finite arc segment in analytical form. Part II: Thin sheet approximation," *IEEE Trans. Magn.*, vol. MAG-18, pp. 911–917, May 1982.

[15] ——, "Vector potential and magnetic field of current-carrying finite arc segment in analytical form. Part III: Exact computation for rectangular cross section," *IEEE Trans. Magn.*, vol. MAG-18, pp. 1860–1867, Nov. 1982.
[16] ——, "Vector potential and magnetic field of current-carrying finite arc segment in analytical form. Part IV: General three-dimensional current density," *IEEE Trans. Magn.*, vol. MAG-20, pp. 2145–2150, Nov. 1984.
[17] ——, "Vector potential and magnetic field of current-carrying finite arc segment in analytical form. Part V: Polygon cross section," *IEEE Trans. Magn.*, vol. 26, pp. 1171–1180, May 1990.
[18] L. Urankar, P. Henninger, and F. S. Nestel, "Compact extended algorithms for elliptic integrals in eletromagnetic field and potential computations. Part 2: Elliptic integral of third kind with extended integration range," *IEEE Trans. Magn.*, vol. 30, pp. 1236–1241, May 1994.
[19] F. W. Grover, *Inductance Calculations, Working Formulas and Tables.* Instrument Society of America, 1973, ch. 18.
[20] S. Pissannetzky, "Structured coils for NMR applications," *IEEE Trans. Magn.*, vol. 28, pp. 1961–1968, July 1992.
[21] W. R. Smythe, *Static and Dynamic Electricity.* New York: McGraw-Hill, 1950.
[22] K. B. Kim, Z. Zabar, E. Levi, and L. Birenbaum, "Restoring force between two non coaxial circular coils," *IEEE Trans. Magn.*, vol. 32, pp. 478–484, Mar. 1996.

Ki-Bong Kim (S'91–M'93) was born in TaeGu, Korea, on November 29, 1956. He received the B.S. degree in electrical engineering from the HanYang University in Seoul, Korea, in 1980, and the M.S. and Ph.D. degrees in electrical engineering from the Polytechnic University, Brooklyn, NY, in January 1990 and June 1993, respectively. His major fields of study at the Polytechnic University were electrical machinery, digital signal processing, and control theory.

He was employed as a Research Associate at the EML Laboratory at the Polytechnic University. Currently he is working on electrical machinery and electronic drives at the SamSung Electronics Co., Suwon, Korea.

Dr. Kim is a member of the KIEE (Korea Institute of Electrical Engineers). He holds six types of electrical engineer's technical licenses from the Korean Government.

Enrico Levi (M'58–SM'58–LS'89) a graduate of the Technion, Haifa, Israel, and received the Ph.D. degree in electrical engineering from the Polytechnic University, Brooklyn, NY.

He is Professor Emeritus of Electrophysics at the Polytechnic University. He has been a visiting professor and has lectured in many universities in the United States and abroad. He has also served as consultant to the U.S. Department of Energy, NASA, the Argonne National Laboratory, the Lawrence Livermore Laboratory, and many industrial firms. His works include *Electromechanical Power Conversion* (1966); *Polyphase Motors: A Direct Approach to Their Design* (1984); chapters in *Magnetohydrodynamic Electric Power Generation* (1978) and *Standard Handbook for Electrical Engineers* (1986), and in the *Encyclopedia of Physical Science and Technology* (1986). He is the author or coauthor of more than 50 papers in technical and scientific journals. He has three patents.

Dr. Levi is a recipient of the Sigma Xi Distinguished Faculty Research Citation, the IEEE Charles J. Hirsch Award, and a Lady Davis Fellowship. He is a member of Tau Beta Pi and Sigma Xi.

Zivan Zabar (S'76–M'81–SM'81) was born in Hadera, Israel, in 1939. He received the B.Sc., M.Sc., and Sc.D. degrees from the Technion–Israel Institute of Technology, Haifa, in 1965, 1968, and 1970, respectively.

He is Head of the Electrical Engineering Department at the Polytechnic University, Brooklyn, NY. His areas of interest are power electronics and electrical power conversion systems. He has five patents and has published more than 50 papers in technical journals.

Dr. Zabar is a member of Sigma Xi.

Leo Birenbaum (S'45–A'48–M'55–SM'70–LS'93) was born in New York City in 1927. He received the B.E.E. degree from the Cooper Union, New York, in 1946, the M.E.E. degree from the Polytechnic Institute of Brooklyn in 1958, and the M.S. degree in physics from the Polytechnic University in 1974.

He is Professor Emeritus at the Polytechnic University where, since 1951, he has worked and published in the areas of microwaves, biological effects of electromagnetic fields, linear motors, and power distribution.

Prof. Birenbaum is a member of the New York Academy of Sciences and the Bioelectromagnetics Society.